Journal Pre-proof

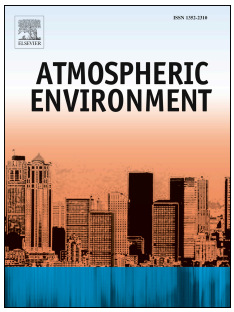

Tropospheric SO_2 and NO_2 in 2012–2018: Contrasting views of two sensors (OMI and OMPS) from space

Yi Wang, Jun Wang

PII: S1352-2310(19)30853-2

DOI: https://doi.org/10.1016/j.atmosenv.2019.117214

Reference: AEA 117214

To appear in: *Atmospheric Environment*

Received Date: 23 July 2019

Revised Date: 11 November 2019

Accepted Date: 6 December 2019

Please cite this article as: Wang, Y., Wang, J., Tropospheric SO_2 and NO_2 in 2012–2018: Contrasting views of two sensors (OMI and OMPS) from space, *Atmospheric Environment* (2020), doi: https://doi.org/10.1016/j.atmosenv.2019.117214.

Jun Wang and Yi Wang: conceptualization, methodology, investigation, writing, reviewing, and editing. Yi Wang: data analysis, visualization, software. Jun Wang: supervision, resources, project administration, funding acquisition.

Tropospheric SO_2 and NO_2 in 2012 - 2018: Contrasting views of two sensors (OMI and OMPS) from space

Yi Wang[1], Jun Wang[1,2]

1. Interdisciplinary Graduate Program in Informatics, The University of Iowa, Iowa City, IA 52242, USA
2. Department of Chemical and Biochemical Engineering, and Center for Global & Regional Environmental Research, The University of Iowa, Iowa City, IA 52242, USA

Correspondences:

Jun Wang (jun-wang-1@uiowa.edu)
Yi Wang (yi-wang-4@uiowa.edu)

Submitted to

Atmospheric Environment
July 2019

Revised
November 2019

Abstract

The global long-term Climate Data Records (CDRs) of atmospheric SO_2 and NO_2 have been obtained from multiple satellite sensors since 1990s, and all these CDRs show consistently decreasing trends in developed countries and increasing trends in developing countries prior to 2010. However, much less clear is the quantitative differences among these CDRs and how such differences affect the inferences for atmospheric SO_2 and NO_2 climatology in terms of their annual means as well as their frequency distributions. Here, we compare and contrast the CDRs from the aged OMI sensor (the flagship for measuring NO_2 and SO_2 since 2005) and the young OMPS sensor series (that started measuring NO_2 and SO_2 in 2012 and will continue in next 2-3 decades). We show that after 2012, the difference of average SO_2 between OMPS and OMI is 0.12 DU and it only decreases to 0.04 DU after bias correction, despite their consistence in spatial pattern. NO_2 CDRs from OMPS and OMI overall exhibit general agreement in both magnitude and spatial pattern between. Furthermore, the CDR differences can lead to the opposite trend signs in developed countries and the difficulty to reconcile trend magnitude in developing countries. Notable consistence in trend signs does exist, regardless of radiative cloud fraction, mainly showing decline of SO_2 and NO_2 in China and increasing in Indian; much inconsistence is, however, found in many parts of developed countries. No SO_2 trends and inconsistent NO_2 trends are found over Europe, and notable differences are found over U.S. where OMI SO_2 and NO_2's declining trends are consistent with surface observations, but OMPS SO_2, albeit its better spatial agreement with surface data, shows increasing trend. This study calls the importance to assess CDRs from different satellite sensors with the account of frequency distributions for extreme events. This importance is emergent as the atmospheric SO_2 and NO_2 amounts are closer to the uncertainties of satellite-based retrievals in developed countries and are or will be declining in developing countries in the coming decades, all of which make the detection of signs, magnitudes, and spatiotemporal dichotomy a challenge from space.

Keywords: SO_2, NO_2, OMPS, OMI, Inconsistent trends

1. Introduction

SO_2 and NO_2 are the largest contributors to anthropogenic aerosols (Seinfeld & Pandis, 2016). Hence, a Climate Data Record (CDR) describing their spatial and temporal variations have shown to be critical to investigate atmospheric composition and climate change especially as a result of aerosol radiative forcing (Myhre et al., 2013). Furthermore, these CDRs have been used to study processes such as emissions (Qu et al., 2017; Streets et al., 2013; Y. Wang et al., 2016), deposition (Liu et al., 2017), transport (Zhou et al., 2012), chemistry (Valin et al., 2013), and trends of atmospheric SO_2 and NO_2 (Kharol et al., 2015; Kharol et al., 2017; Krotkov et al., 2016; Lamsal et al., 2015; Andreas Richter et al., 2005; Zhou et al., 2012). Here, according to National Research Council (2014), CDR is defined as "a time series of measurements of sufficient length, consistency and continuity to determine climate variability and change", and hence, anthropogenic climate change is an inherent part of the CDR.

Satellites have been providing observation-based global SO_2 and NO_2 CDRs for more than two decades, which contrasts with ground in situ observational sites that are sparse and unevenly distributed in space. The global tropospheric Vertical Column Density (VCD) distributions of SO_2 and NO_2 were first retrieved by Global Ozone Monitoring Experiment (GOME) during 1996-2004 (Burrows et al., 1999; Lee et al., 2009; Martin et al., 2002), and are subsequently continued by two GOME-2 sensors since 2006 and 2011, respectively (Munro et al., 2016; Nowlan et al., 2011; A. Richter et al., 2011), by SCanning Imaging Absorption SpectroMeter for Atmospheric CHartographY (SCIAMACHY) during 2002-2012 (Bovensmann et al., 1999; Lee et al., 2009), by Ozone Monitoring Instrument (OMI) since 2004 (Krotkov et al., 2017; Li et al., 2013), by two Ozone Mapping and Profiler Suite (OMPS) sensors since 2011 and 2017,

73 respectively (Yang et al., 2014; Yang et al., 2013), and by TROPOspheric Monitoring Instrument
74 (TROPOMI) since 2017 (Veefkind et al., 2012). The third OMPS is scheduled to launch in 2022
75 and will extend the long-term CDRs of SO_2 and NO_2 for the next 2-3 decades.

76 Observations from GOME, GOME-2, SCIAMACHY, and OMI have been widely applied to
77 estimate SO_2 and NO_2 trends. However, in most past studies, only CDRs from single sensor were
78 used to study corresponding SO_2 and NO_2 trend during the sub-period (usually no more than 10
79 years) of the past two decades, and the results varied by region and time period (Kharol et al.,
80 2015; Kharol et al., 2017; Krotkov et al., 2016; Lamsal et al., 2015; Schneider et al., 2015;
81 Schneider & van der A, 2012; Zhou et al., 2012). For studies that using CDRs from two or more
82 sensors, with or without adjusting bias among CRDs, little attention was paid to quantitatively
83 compare difference of these CDRs for their overlapped time period (Georgoulias et al., 2019;
84 Ghude et al., 2009; Hilboll et al., 2013; Lin et al., 2019; Richter et al., 2005; van der A et al.,
85 2006), or only focus on strong polluted regions (Zhang et al., 2017).

86 Despite the progress in trend analysis of SO_2 and NO_2 from GOME, GOME-2, SCIMACHY,
87 and OMI CDRs, outstanding questions remain especially regarding the consistencies or
88 differences of trend sign and magnitude detected by different sensors, the impacts of cloud on
89 trend detection, and the change of frequency distribution or probability density functions for both
90 species that include not only mean, but also median and extreme values. Addressing these issues
91 is critical due to three factors. Firstly, emission decline at slower pace over developed countries
92 (Jiang et al., 2018) is expected to make weak trend signals that may or may not be consistently
93 described by different satellite CDRs, which has not been revealed in literature. Secondly, SO_2
94 and NO_2 CDRs are usually retrieved under all-sky conditions while the impact of cloud cover
95 selection on trend detection is still unclear. Thirdly, past researches focused on analyzing trends

of monthly or yearly mean rather than evolution of frequency of extreme SO_2 and NO_2 event while the latter is more meaningful for air quality scientific community. These problems are compounded as trend analysis of NO_2 and SO_2 after 2010 may be subject to large uncertainties caused by row anomalies (Schenkeveld et al., 2017) in aged OMI as well as that large differences in overpassing times of GOME, SCIMACHY and GOME-2 against OMI, which ultimately lead to no temporal overlaps with OMI. Fortunately, OMPS started observations in 2012 with similar overpassing time of OMI, and in this work, we make the first attempt to address these issues by using concurrent measurements of tropospheric VCD of SO_2 and NO_2 from OMI and OMPS during April 2012 – July 2018.

2. Data and Methods

2.1 Data

OMI and OMPS VCD products for SO_2 and NO_2 from NASA are used in this study, and their detailed description is provided in S1 and S2. Briefly, OMI SO_2 retrieved by means of principal component analysis have the precision of 0.5 DU (1 DU = 2.69×10^{16} molecules cm^{-2}) (Li et al., 2013), which is a factor of 2.5 lower than that of OMPS SO_2 (0.2 DU) retrieved through Direct Vertical Column Fitting (DVCF) algorithm (Yang et al., 2013). The better precision of OMPS SO_2 is possibly caused by the fact that OMPS use a single detector array to cover 310 nm, where strong SO_2 absorption exists, while the band is not used in OMI SO_2 retrieval due to channel split near 310 nm for OMI (Yang et al., 2013). OMI and OMPS NO_2 are retrieved through variation of differential optical absorption spectroscopy algorithm (Krotkov et al., 2017) and DVCF (Yang et al., 2014), respectively. Although the precision of NO_2 total slant column density is about 0.033 DU for both OMPS and OMI, tropospheric VCD precision is 0.011 DU for OMPS, which

is better than 0.017 DU for OMI (Krotkov et al., 2017; Yang et al., 2014). The precision difference between OMPS and OMI tropospheric NO_2 VCD is caused by different Stratosphere-Troposphere Separation (STS) approaches; OMI STS approach uses a small window to smooth stratospheric VCD, leaving some intrinsic measurement noise in the tropospheric VCD (Yang et al., 2014).

Ground-based daily SO_2 and NO_2 measurements are obtained from U.S. EPA's Air Quality System Data Mart (https://www.epa.gov/airdata). SO_2 is measured through coulometry or UV fluorescence methods, and NO_2 is observed by chemiluminescence approach (Demerjian, 2000). The NO_2 observational method actually measures NO by decomposing NO_2 to NO, which could systematically lead to positive bias, as NO_z (all compounds that are products of the atmospheric oxidation of NO_x) will be also reduced to NO (Lamsal et al., 2015). However, the systematic positive has very small impacts on relative trend values (Silvern et al., 2019), let alone the sign of trend.

2.2 Methods

The OMI Level-3 SO_2 and NO_2 products at 0.25°x0.25° grids are preprocessed to construct monthly mean datasets at 1°x1° grids through "drop-in-the-box" gridding method (Sun et al., 2018). 1°x1°, instead of 0.25°x0.25° grids are used as OMPS pixel size (50 km x 50 km at nadir) is much larger than 0.25°x0.25° grids. In the OMI Level-3 products, only the pixels that are not affected by row anomalies and have little cloud contamination, or Radiative Cloud Fraction

(RCF) < 0.2 and 0.3 for SO_2 and NO_2, respectively, are retained. To remove the impacts of transient SO_2 cloud, only retrievals that are less than 15 DU are used, although passive volcanic degassing signals still exists. In the research, we mainly focus on China, India, the U.S., Europe, equatorial Pacific ocean (10°S–10°N,120°W–150°W), to where volcanic sources do not contribute SO_2 except southern Europe (SO_2 source distribution is available at https://so2.gsfc.nasa.gov/). The same gridding approach and RCF thresholds are applied to OMPS SO_2 and NO_2 except in the investigation of how cloud affects trends, in which RCF thresholds vary.

Trend analysis approach introduced by Weatherhead Elizabeth et al. (1998) is applied to all CDRs as well as in situ observations. This method not only detects linear trend with consideration of seasonal variabilities and noise, but also conduct statistical significant test of it. The linear trend analysis model is shown as

$$Y_t = \mu + S_t + \omega X_t + N_t \qquad t = 1, 2, \dots, T \qquad (1)$$

where Y_t is monthly mean time series of observational variables (SO_2 or NO_2), μ is the offset at the start of time series, T is the total number of month, $X_t = t/12$ is number of years, ω is the magnitude of linear trend per year, $S_t = \sum_{j=1}^{4}\left[\beta_{1,j}\sin(2\pi jt/12) + \beta_{2,j}\cos(2\pi jt/12)\right]$ represents seasonal variations, and N_t is noise that cannot be represented by the model. N_t is assumed as red noise and represented as $N_t = \phi N_{t-1} + \varepsilon_t$, where ϕ is the autocorrelation between N_t and N_{t-1} and ε_t is white noise. The standard deviation of the yearly linear trend is represented as

$$\sigma_\omega = \frac{\sigma_N}{n^{3/2}}\sqrt{\frac{1+\phi}{1-\phi}} \qquad (2)$$

where σ_N is the standard deviation of N_t, and n equals $T/12$. If the absolute value of ω/σ_ω is larger than 2, it indicates that the linear trend is at 95% confidence level.

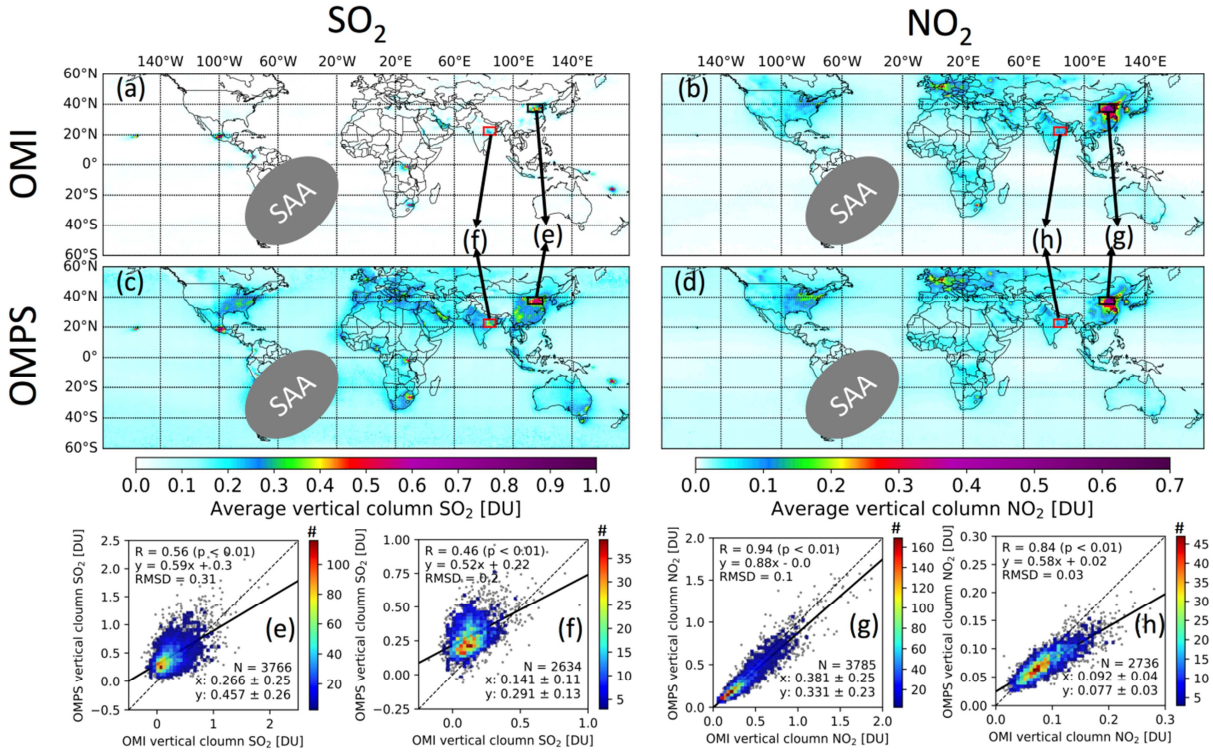

Figure 1. Averages VCD of OMI SO_2 (a) and NO_2 (b) and OMPS SO_2 (c) and NO_2 (d) during April 2012 - July 2018. South Atlantic Anomaly (SAA) region is masked by grey ellipse. (e) and (f) are scatter plots of monthly average of OMPS SO_2 versus OMI SO_2 over North China plain (black box) and Eastern India (red box), respectively. (g) and (h) are similar to (e) and (f), respectively, but for NO_2. Also shown on the scatter plots are 1:1 line (dash), linear regression line (solid), linear regression formula, Pearson correlation coefficient (R), p-value (p), root mean squared difference (RMSD), number of collocated pairs (N), OMI average and standard deviation (x), OMPS average and standard deviation (y), and density of collocated pairs (colorbar).

3. Results

Global distributions of SO_2 and NO_2 from OMI and OMPS during April 2012 - July 2018 are shown in figure 1. OMI and OMPS observe similar patterns with the largest SO_2 level over China and India, followed by Europe, and the U.S., and the largest NO_2 level over China, followed by Europe, the U.S., and India. OMPS SO_2 VCD in global average is 0.129 DU, which

is much larger than 0.004 DU of OMI, and the NO_2 difference is smaller with OMPS and OMI NO_2 0.023 DU and 0.017 DU, respectively. Despite good agreement in qualitative description of spatial distribution for both SO_2 and NO_2, OMI and OMPS CDRs have significant differences in the magnitudes and trends at regional scale during April 2012 - July 2018 (figure 2).

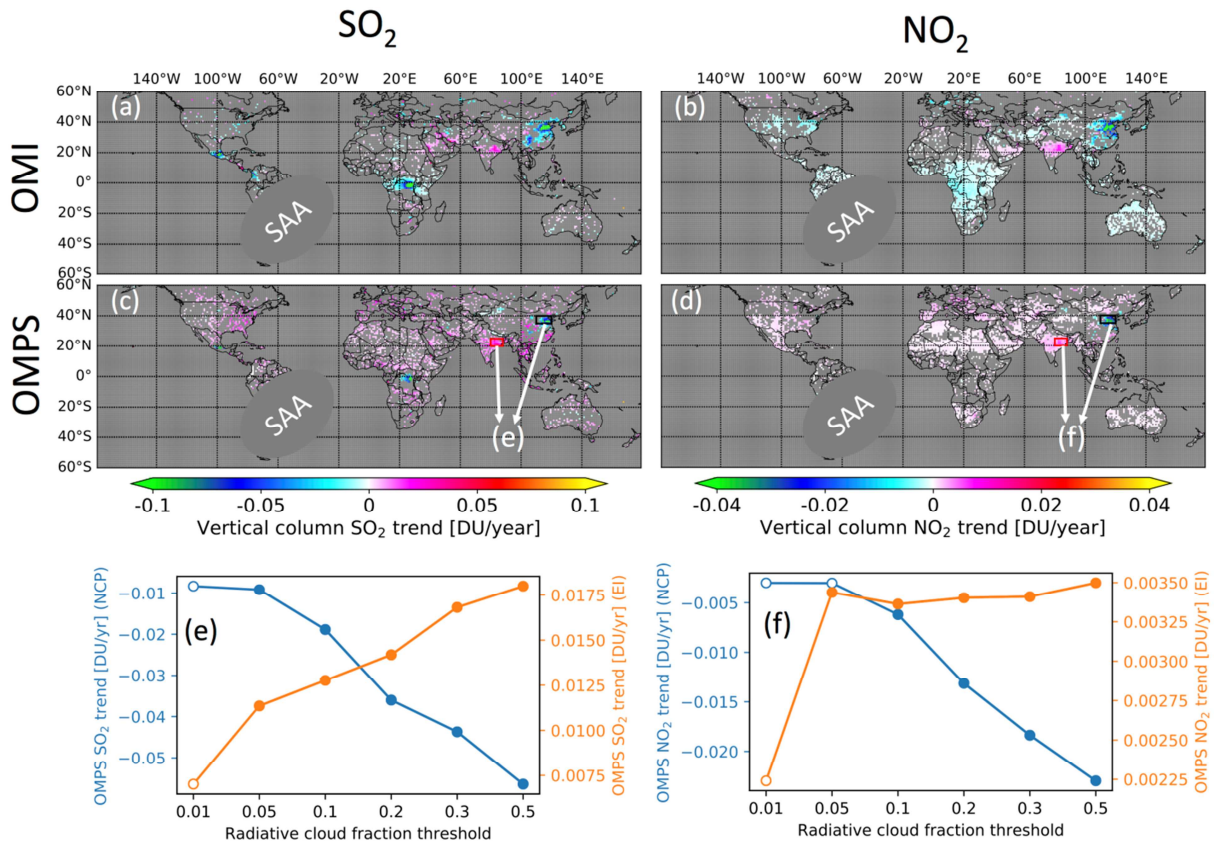

Figure 2. Trends of VCD of OMI SO_2 (a) and NO_2 (b) and OMPS SO_2 (c) and NO_2 (d) during April 2012 - July 2018. Only pixels that show trends at 95% confidence level and over land are shown. South Atlantic Anomaly (SAA) region is masked by grey ellipse. (e) and (f) are trends of OMPS SO_2 and NO_2, respectively, over North China Plain (NCP) and Eastern India (EI) at various radiative cloud fraction thresholds. Trends that are at 95% confidence level and not are shown by solid circles and open circles, respectively.

3.1 China and India

Consistent are the locations of hot spots for SO_2 and NO_2 over China and India (figure 1a-d), the two largest anthropogenic SO_2 and NO_x emitters in Asia (Janssens-Maenhout et al., 2015). Both OMI and OMPS observe the largest SO_2 loadings over the North China Plain (NCP), Sichuan basin (30° N, 105° E), and Eastern India (EI) (figure 1a and 1c). As to NO_2, hot spots are over NCP, the Yangtze River Delta (megacity clusters), Sichuan basin, the Pearl River Delta (megacity clusters), EI, and New Delhi, India's capital (figure 1b and 1d).

Though consistent qualitatively, tropospheric VCD of SO_2 and NO_2 from the two sensors over NCP and EI show systemic differences quantitatively. The averages of OMPS SO_2 are 0.46 DU and 0.30 DU over the NCP and EI, respectively, which contrast with lower values of 0.27 DU and 0.14 DU for OMI (figure 1e and 1f), and pearson correlation coefficients (R) of OMI and OMPS monthly mean SO_2 at 1°x1° grid cell are 0.56 (figure 1e) and 0.46 (figure 1f) over NCP and EI, respectively. OMPS shows stronger SO_2 seasonal variability than OMI with coefficient of variation (standard deviation over average) of monthly mean 0.34 and 0.33 over NCP and EI, respectively, which are much larger than 0.16 and 0.25 for OMI (figure 3). Unlike large SO_2 difference between OMI and OMPS, averages of OMI NO_2 retrievals over the NCP and EI are 0.38 DU (figure 1g) and 0.09 DU (figure 1h), respectively, only slightly larger than OMI counterparts of 0.33 DU (figure 1g) and 0.08 DU (figure 1h). Moreover, R of monthly averaged NO_2 between OMI and OMPS are large as 0.94 (figure 1g) and 0.84 (figure 1h) over the NCP and EI, respectively. Comparable seasonal variability of NO_2 is detected by the two sensors over NCP (coefficient of variation of 0.43 and 0.47 for OMI and OMPS, respectively) as well as EI (coefficient of variation of 0.22 and 0.21 for OMI and OMPS, respectively) (figure 3).

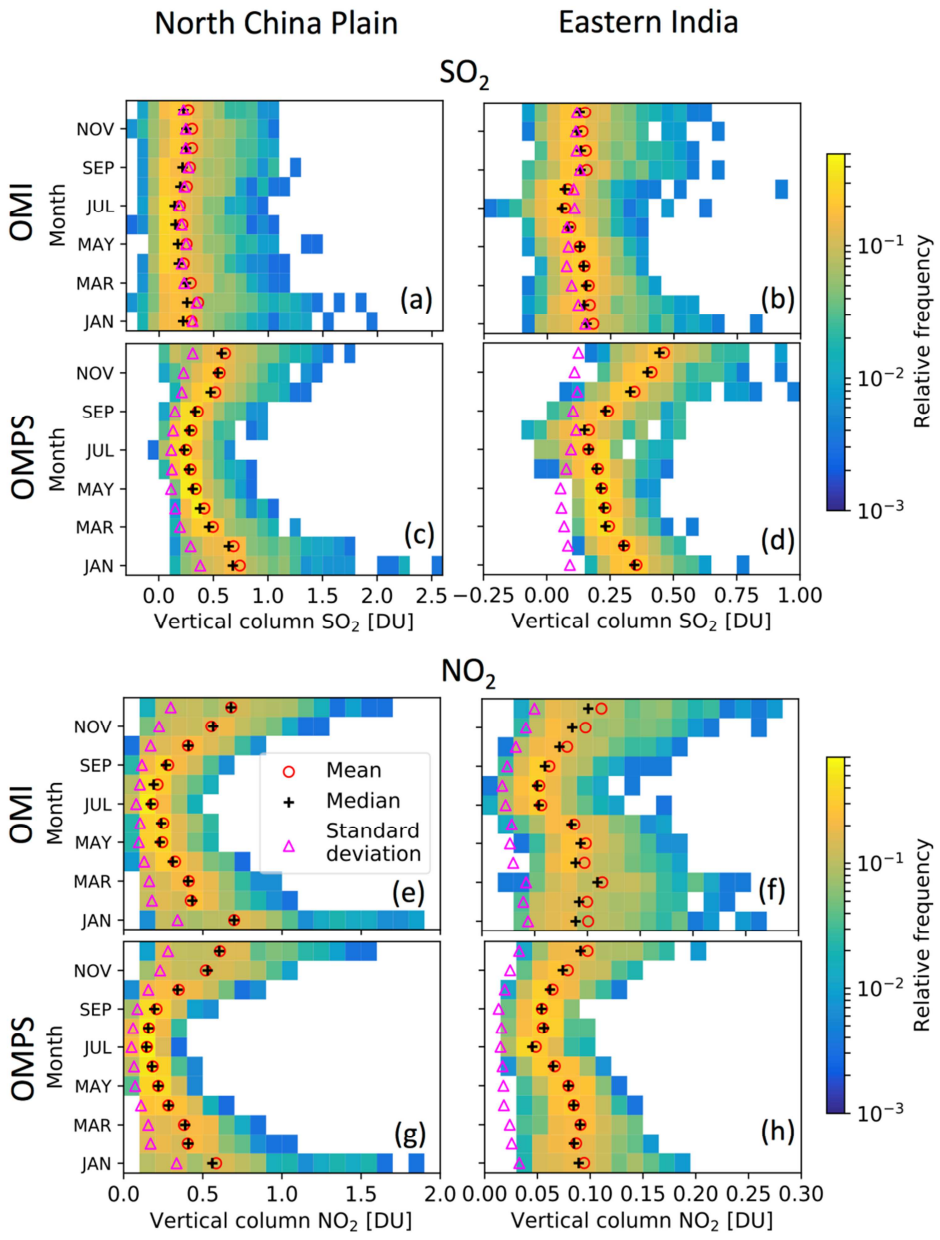

Figure 3. (a) and (c) are relative frequency of OMI and OMPS SO_2 vertical column density (regrided in 1°x1° gridbox) as a function of month over Northern China Plain (black box in figure 1) during April 2012 - March 2018, respectively. (b) and (d) are similar to (a) and (c), respectively, but for Eastern India (red box in figure 1). (e)-(h) are similar to (a)-(d), respectively, but for NO_2.

Despite systematic differences, OMI and OMPS SO_2 and NO_2 retrievals constantly show decreasing trends over China and increasing trends over India (figure 2a-d). Downward SO_2 trends

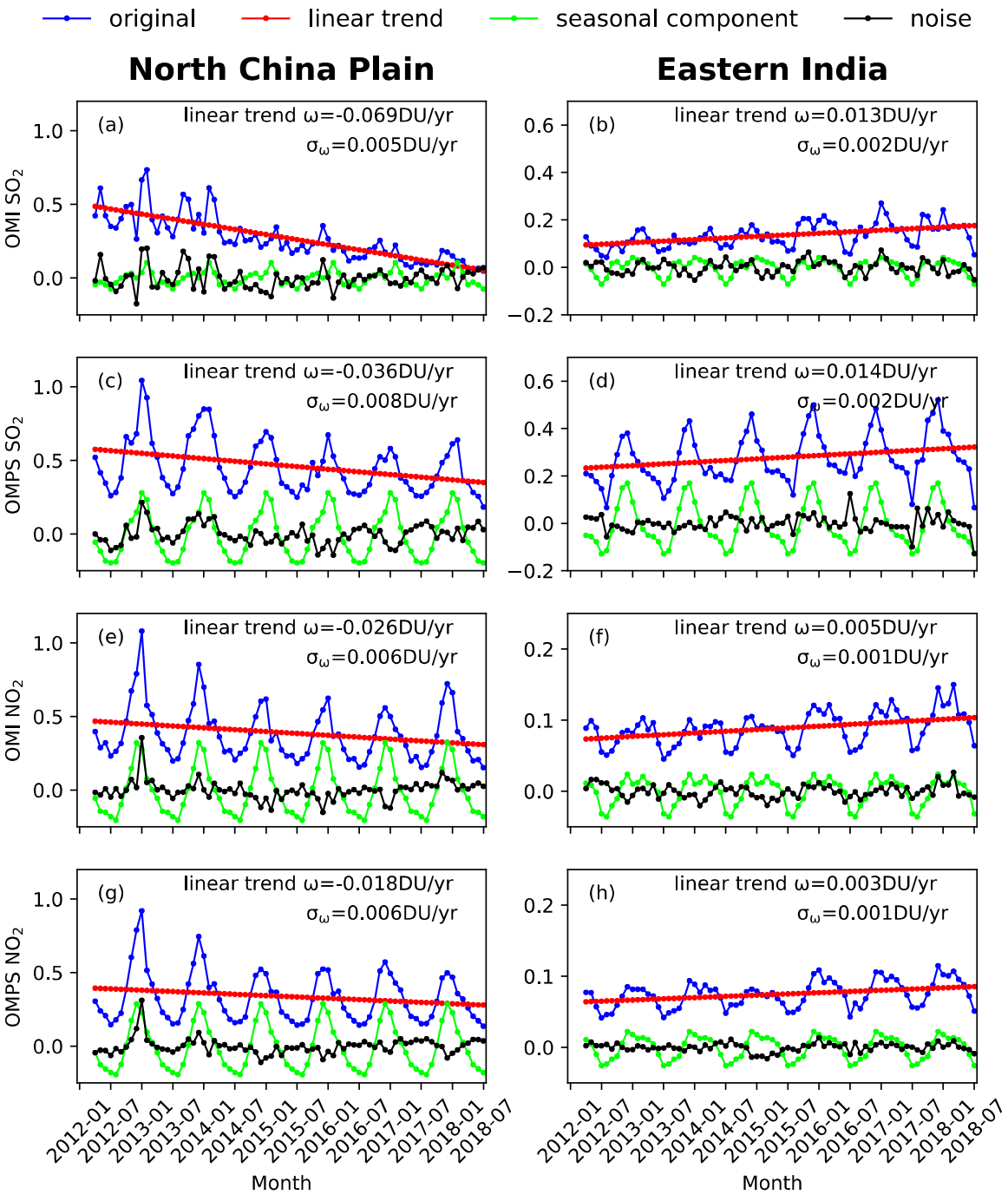

Figure 4. Time series of monthly SO_2 and NO_2, and their decompositions over Northern China Plain (black box in figure 1) and Eastern India (red box in figure 1). (a) and (c) are SO_2 over Northern China Plain from OMI, OMPS, respectively. (e) and (g) are similar to (a) and (c) but for NO_2. (b), (d), (f), and (h) are similar to (a), (c), (e), and (g) but for Eastern India. Satellite vertical column density (blue line) is decomposed into linear trend (red line), seasonal component (green line), and noise (black line). Linear trend ω and its standard deviation σ_ω are shown.

are observed by both OMI and OMPS over the NCP (-0.069 DU/yr for OMI and -0.036 DU/yr for OMPS, shown in figure 4), the Sichuan basin (30° N, 105° E), and Xingjiang province (43° N, 85° E), although OMI detects more pixels with decreasing trends than OMPS (Figure 2a and 2c).

Over EI, both OMI and OMPS SO_2 retrievals observe upward trends (0.013 DU/yr for OMI and 0.014 DU/yr for OMPS, shown in figure 4), while OMPS detects more pixels with increasing trends than OMI (Figure 2a and 2c). The contrasting SO_2 trends between NCP and EI could be a result of much higher rate of installation and operation of flue gas desulfurization over China than India (Krotkov et al., 2016; S. Wang et al., 2015). Moreover, India not only has overtaken U.S. as the world's second largest SO_2 emitting country in 2014 (Krotkov et al., 2016) but also is surpassing, if not already, China to be the world's largest SO_2 emitter in 2016 (Li et al., 2017), which is reflected by the downward trends over NCP and upward trends over EI that are detected by both OMI and OMPS. As for NO_2, both sensors observe strong decreasing trends over the NCP (-0.026 DU/yr for OMI and -0.018 DU/yr for OMPS, shown in figure 4), although OMI observes the weak downward trends that are not detected by OMPS over parts of Southern China (Figure 2b and 2d). The penetration of denitration devices for coal-fired power plants and strict regulation for vehicle emissions should be primary reasons for these reductions (Fei et al., 2016). Conversely, stronger upward trends of NO_2 over EI (0.005 DU/yr for OMI and 0.003 DU/yr for OMPS, shown in figure 4) than Western India are detected by both OMI and OMPS (figure 2b

247 and 2d), which should be mainly ascribed to the increasing fuel consumption of coal-fired power
248 plants without emission regulation (Krotkov et al., 2016).

249 Trends signs detected by OMPS are independent of RCF, but trend magnitudes are positively
250 correlated with RCF. OMPS SO_2 (NO_2) trends change from -0.008 DU/yr (-0.003 DU/yr) to -
251 0.056 DU/yr (-0.023 DU/yr) over NCP and from 0.007 DU/yr (0.0022 DU/yr) to 0.018 DU/yr
252 (0.0035 DU/yr) over EI as RCF threshold increases from 0.01 to 0.5, and all these trends are at
253 95% confidence level when RCF threshold is no less than 0.1 (figure 2e-f).

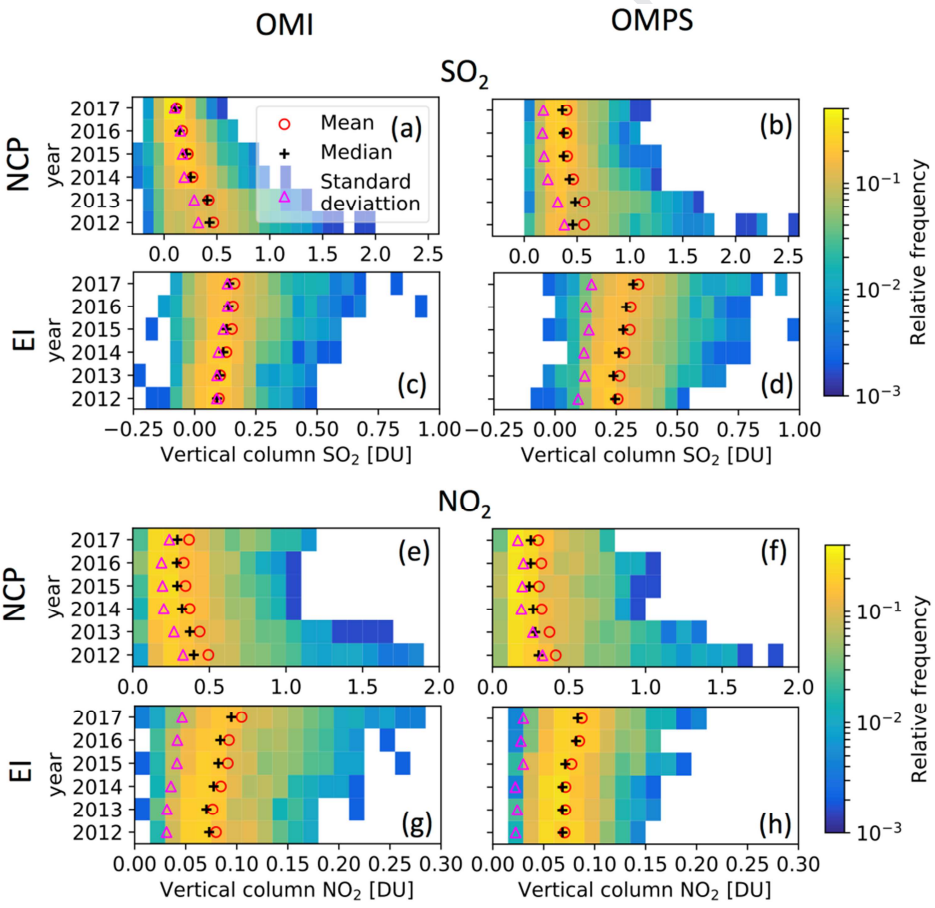

254

255 Figure 5. (a) and (b) are relative frequency of OMI and OMPS SO_2 vertical column density
256 (regrided in 1°x1° gridbox) as a function of year over Northern China Plain (NCP, black box in
257 figure 1) during April 2012 - March 2018, respectively. (c) and (d) are similar to (a) and (b),

respectively, but for Eastern India (EI, red box in figure 1). (e)-(h) are similar to (a)-(d), respectively, but for NO_2.

To investigate the trends of extremely high monthly mean SO_2 and NO_2 loading, relative frequency distribution of the two trace gases over NCP and EI as a function of year are shown in figure 5. Over NCP, OMI and OMPS SO_2 maximums reduce from ~2.0 DU and ~ 2.6 DU in 2012 to ~0.6 DU and ~1.2 DU in 2017, respectively (figure 5a and 5b), in contrast to Eastern India, where they increase from ~0.50 DU and ~0.55 DU to ~0.85 DU and ~0.95 DU, respectively (figure 5c and 5d). Not only OMI and OMPS SO_2 loading averages and medians show downward (upward) trends over NCP (EI), but also the relative frequencies of SO_2 larger than 0.5 DU decrease from 42.7% (47.1%) in 2012 to 0.2% (24.7%) in 2017 for OMI (OMPS) over NCP and increase from 0.0% (0.2%) to 2.9% (11.8%) over EI (figure 5a-d). As for NO_2, maximums of both OMI and OMPS are ~1.9 DU in 2012, reducing to ~1.2 DU and ~0.8 DU in 2017, respectively, over the NCP (figure 5e and 5f); conversely, they increase from ~0.17 DU and ~0.15 DU to ~0.27 DU and ~0.21 DU, respectively, over EI (figure 5g and 5h). Moreover, decreasing trends of NO_2 averages and medians over NCP and increasing trends over EI are also observed by the two sensors. Relative frequencies of NO_2 larger than 0.5 DU are 23.0% and 14.8% in 2017, down from 36.3% and 27.7% in 2012 for OMI and OMPS, respectively, over NCP, while NO_2 loadings over EI are constantly less the 0.5 DU. If the threshold is 0.15 DU, relative frequencies over EI rise from 2.7 % and 0.0% to 16.0% and 3.5% for OMI and OMPS, respectively.

3.2 U.S.

In contrast to overall consistent finding over China and India, the averages of OMI and OMPS SO_2 retrievals sampled at EPA sites as well as their trends are quite different. EPA in situ SO_2 observations show hot spots over Illinois, Indiana, Ohio, and Pennsylvania states (figure 6a), where OMPS (figure 6b) also detects large SO_2, while OMI (figure 6c) does not. Moreover, the spatial R between OMPS SO_2 retrievals and EPA in situ SO_2 observations is 0.27 ($p<0.01$) while there is no correlation between OMI retrievals and EPA observations ($R=0.08$, $p>0.05$). OMPS SO_2 retrievals are in the range of 0.08 to 0.35 DU (figure 6c) which are much larger than OMI counterparts of being less than 0.07 DU. Although many EPA sites over eastern U.S. show decreasing trends of SO_2 (figure 6d), OMI detects only downward trends at a small number of EPA sites over eastern U.S. and both upward and downward trends are detected by OMPS.

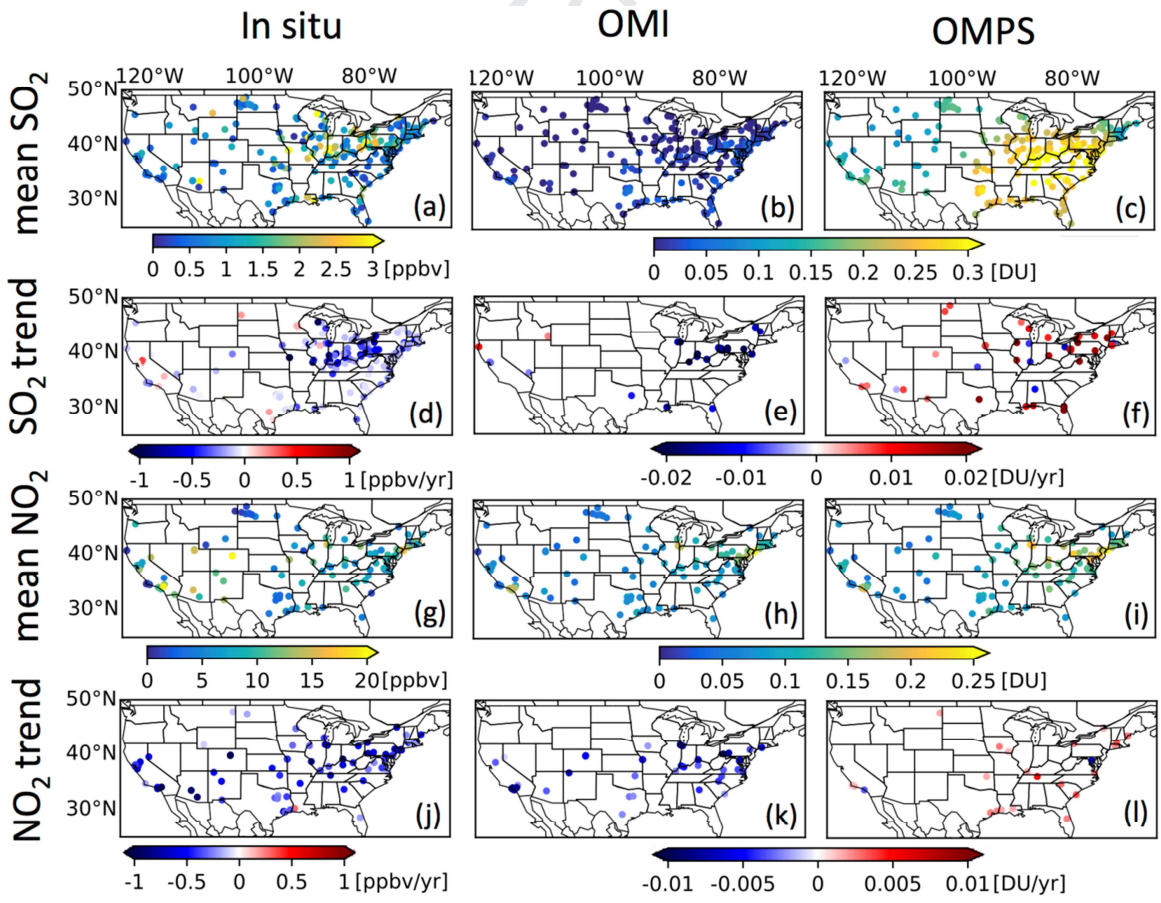

Figure 6. (a) is averages of EPA in situ SO_2 during April 2012 - December 2017. (b) and (c) are averages of OMI and OMPS SO_2 VCD sampled at EPA sites, respectively. (d), (e), and (f) are trends of EPA in situ SO_2, OMI SO_2 VCD and OMPS SO_2 VCD, respectively. (g)-(l) are similar to (a)-(f), but for NO_2. Only sites that show trends at 95% confidence level are plotted.

The typical SO_2 levels over the U.S. are quite low, and likely below the detection limit of OMI SO_2 retrieval algorithm, as illustrated by the lack of spatial correlation between OMI SO_2 and EPA in situ observations. While both OMI and OMPS have very stable performance over time with less than 0.5% degradation per year, long-term trends over regions with low SO_2 concentrations determined from OMI and OMPS retrievals may be impacted by small instrumental changes (Schenkeveld et al., 2017; Seftor et al., 2014), which have not yet been corrected in the OMI and OMPS products used in this investigation.

For NO_2, the averages of OMI and OMPS retrievals sampled at EPA sites are similar, while their trends are quite different. EPA observations, OMI retrievals, and OMPS retrievals all detect NO_2 hotspots around Los Angeles, Chicago and New York (figure 6g-i); the spatial R for EPA in situ observations with OMI and OMPS retrievals are 0.61 ($p<0.01$) and 0.50 ($p<0.01$), respectively. OMI and EPA consistently show decreasing trends; conversely, OMPS detects increasing trends.

3.4 Europe

OMPS SO_2 is larger than OMI over Europe, and neither of the two products shows significant trend. OMPS SO_2 is in the range of 0.15 to 0.25 DU (figure 1c) over almost all the Europe, which contrasts to the small value of less than 0.1 DU for OMI (figure 1a). OMPS observes large SO_2 levels over England, Bosnia and Herzegovina, Serbia, and Bulgaria, where large coal-fired power plants exist (Fioletov et al., 2016), and OMI also detects these hot spots except England.

There are, however, no significant trend observed by either of the two products over these countries.

For NO_2, OMI and OMPS show a similar spatial pattern over Europe while trends are not always in accord. OMI and OMPS observe NO_2 hot spots around metropolises which include Manchester, Liverpool, and London in England, Amsterdam in Netherlands, Brussels in Belgium, Cologne, Frankfurt, and Berlin in Germany, Paris in France, and Moscow in Russia, and industrial areas around Milan in Italy and Katowice in Poland (figure 1b and 1d). Decreasing trends over areas around London in England, Amsterdam in Netherland, Brussels in Belgium, Cologne and Frankfurt in German, Milan in Italy are detected by OMI while OMPS does not show trends in those regions (figure 2b and 2d). Both instruments, however, observe enhanced NO_2 levels over western Turkey (figure 2b and 2d).

4. Discussion

SO_2 and NO_2 tropospheric VCD retrievals from OMI and OMPS are compared, which reveals their inconsistencies at different regions and seasons. Discussion of several factors that may or may not cause the differences of loadings and trend signs of SO2 and NO2 from both an algorithm and sensor characteristics point of view are provided below.

First, some differences can be explained by analyzing the bias and trends over the clean equatorial Pacific ocean (10°S–10°N,120°W–150°W) where averages and trends of SO_2 and NO_2 are expected to be zero. Thus, the non-zero averages and trends are considered as systematic artifacts inherent in the algorithm. Positive OMPS SO_2 trends widely exist over remote clean ocean (Figure S1c in the supporting information), and a positive trend of 8.9×10^{-4} DU/year (Figure S2b) even exist over the clean equatorial Pacific ocean; in contrast, OMI

observes both positive and negative SO_2 trends randomly exist over remote clean ocean (Figure S1a), and the positive trend of $7.3x10^{-5}$ DU/year (Figure S2a) over the clean equatorial Pacific ocean for OMI is much less than that derived from OMPS. For NO_2 over clean ocean, OMPS retrievals generally show positive trends (Figure S1d), while OMI retrievals overall show negative trends (Figure S1b); the NO_2 trends are $7.4x10^{-5}$ DU/year for OMPS (Figure S2d) for OMI and $-1.0x10^{-4}$ DU/year (Figure S2c) for OMI. Thus, the positive SO_2 and NO_2 trends (artifacts) derived from OMPS may partly explain why (a) inconsistent NO_2 trends are found over Europe and (b) notable differences are found over U.S. where OMI SO_2 and NO_2's declining trends are consistent with surface observations, but OMPS SO_2, albeit its better spatial agreement with surface data, shows increasing trends.

Second, averages of SO_2 over the clean equatorial Pacific ocean (10°S–10°N,120°W–150°W) are 0.0035 DU for OMI and 0.0789 DU for OMPS (Figure S2), and these values are considered as systematic bias. The differences of average SO_2 between OMPS and OMI are 0.12 DU globally and 0.2 DU over Eastern China; their counterparts, after bias correction, decrease to 0.04 DU and 0.12 DU respectively. Bias correction partly helps to reconcile the two products, but the large differences still exist.

Third, NO_2 fitting windows are 345-378 nm for OMPS and 402-465 nm for OMI, but such difference is not expected to lead to inconsistent NO_2 trends over the US and Europe between OMI and OMPS. OMI NO_2 Slant Column Density (SCD) is retrieved by a DOAS approach and it is converted to VCD by a AMF. The OMI NO_2 AMF is assumed to be wavelength-independent. This assumption could lead to errors in the VCD, but we don't expect the error can change the sign of NO_2 trend. OMPS NO_2 is retrieved through Direct Vertical Column Fitting

(DVCF) algorithm. In the DVCF approach, average AMF (or photon path lengths) for each wavelength (, which is implicitly determined in the spectral fitting process) is used. Thus, for OMPS NO_2 VCD, wavelength-dependent of AMF is considered, and this is a key improvement of the DVCF approach over the DOAS method (Yang et al., 2014). However, DVCF method itself presumably won't lead to statistically significant trend in the retrieval products.

Fourth, aerosols are not considered in AMF calculation by the algorithms generating the data used in this study. This simplification may affect trend strength to some extent. McLinden et al. (2016) estimated that uncertainty of AMF due to aerosols is 10% by adjusting aerosol optical depth of ±0.25 and recalculating AMFs. Considering AOD trends are less than 0.04 per year (or 0.25 during April 2012 - July 2018) almost everywhere (except some regions over China and Western Asia) (Figure S3), we can expect that the impact aerosol loading on SO_2 and NO_2 trends are less than 10% at most locations, which doesn't change the key results of our findings.

Finally, both systematic bias and random error can also be introduced in the SO_2 retrievals due to O_3 interference, which may affect trend analysis. Trends derived over the clean equatorial Pacific ocean (10°S–10°N,120°W–150°W) (Figure S2) can be considered as the lower limit of systematic bias over other regions. In the trend analysis, time series of original retrievals are decomposed into linear trend, seasonal component, and noise. The random error due to O_3 interference is expected in the noise part, thus they should not affect trend estimations, but affect standard deviations of trend.

In summary, the user guides for OMPS and OMI SO_2 and NO_2 data are used in our analysis, and so, a thorough analysis of the algorithm differences that contribute to the product difference is out the scope of this study that has a primary focus on the data analysis. For OMPS Level-2 product, we only use data labeled as good pixel. Data quality control has been applied to in generation of OMI Level-3 product from its Level-2 data, and here; all OMI Level-3 data are considered as good. Nevertheless, to reconcile the differences of SO_2 and NO_2 CDRs from different sensors and algorithms, algorithm inter-comparison studies supplemented with ground-based observations for validating the data products are needed.

5. Conclusions

Satellite-based CDRs for atmospheric SO_2 and NO_2 play an increasingly significant role in trend analysis. We compared CDRs of SO_2 and NO_2 tropospheric VCD retrievals from OMI and OMPS during their overlapped period (2012-2018) and showed their consistencies and inconsistencies. The two sensors observe similar spatial distribution of SO_2 and NO_2 globally. OMPS SO_2 is much larger than OMI SO_2 in global average, while NO_2 difference is much smaller than SO_2 difference. The inconsistencies among CDRs can be caused by differences in sensors, calibration procedures, sampling processes, retrieval algorithms and spatial aggregation/averaging approaches (Levy et al., 2015), which should be addressed in future studies. The differences of magnitudes and trends observed by the two sensors vary by region.

Both OMI and OMPS observe large SO_2 and NO_2 levels over North China Plain as well as Eastern India, although OMI SO_2 is systemically lower than OMPS. Despite magnitude variation between OMI and OMPS, downward (upward) trends of mean, median, maximum, and the frequency of extreme event for SO_2 and NO_2 are detected by the two sensors over North China

Plain (Eastern India). Radiative cloud fraction has no impact on trend signs, but is positively correlated with trend magnitudes.

OMI and OMPS NO_2 are spatial correlated with EPA in situ surface measurements over the U.S., but for SO_2, only OMPS shows significant spatial correlation with EPA. Downward trends of SO_2 and NO_2 are found by OMI, which are consistent with EPA surface observations, while OMPS mainly show upward trends for both SO_2 and NO_2. Over Europe, SO_2 and NO_2 hot spots are observed by OMI and OMPS over metropolises and industrial areas. Although both show no SO_2 trends, OMI and OMPS NO_2 trends are not always in accord with each other.

Surface SO_2 and NO_2 levels have become low and stable in some regions of the U.S. and Europe. As a result, future research should focus on local areas around their sources, hence requiring data with higher spatial resolution. TROPOMI (Veefkind et al., 2012) was launched in 2017 and would provide SO_2 and NO_2 retrievals with higher spatial resolution (7 km x 3.5 km) than both OMI (13km x 24 km) and OMPS (50km x 50 km). Considering the short lifetime of SO_2 and NO_2 in the troposphere, the importance of satellite observations will be enhanced by the launch of geostationary satellites which includes TEMPO (Zoogman et al., 2017) monitoring North America, Sentinel-4 (Ingmann et al., 2012) monitoring Europe, and GEMS (Kim, 2012) monitoring Eastern Asia in the near future. All these advancements will provide hourly SO_2 and NO_2 retrievals during daytime with high spatial resolution (2.1 km x 4.4 km for TEMPO, 8.9 km x 11.7 km for Sentinel-4, and 7 km x 8km for GEMS). These high-resolution data enable an unprecedented opportunity to investigate SO_2 and NO_2 variability in different spatiotemporal scale, thereby providing benchmarks to address OMPS-OMI trend differences revealed in this study, especially those over developed countries where pollutant levels are low and trend signals (if any) can be difficult to be sensed by the current generation of satellite sensors.

ACKNOWLEDGEMENTS

This work was supported by NASA Aura Science Team and Atmospheric Modeling and Analysis program (grant #: NNX17AF63G managed by Dr. Kenneth Jucks and Dr. Richard Eckman) as well as TEMPO (Tropospheric Emissions: Monitoring of Pollution) satellite mission. Satellite data and in situ data shown in the paper can be obtained from NASA (https://disc.gsfc.nasa.gov/) and EPA (https://www.epa.gov/outdoor-air-quality-data), respectively. The results presented in this manuscript will be made available through Coalition on Publishing Data in the Earth and Space Sciences (https://copdessdirectory.osf. io) and please email J. Wang (jun-wang-1@uiowa.edu) for details.

Reference

Bovensmann, H., Burrows, J. P., Buchwitz, M., Frerick, J., Noël, S., Rozanov, V. V., et al. (1999). SCIAMACHY: Mission Objectives and Measurement Modes. *Journal of the Atmospheric Sciences, 56*(2), 127-150.

Burrows, J. P., Weber, M., Buchwitz, M., Rozanov, V., Ladstätter-Weißenmayer, A., Richter, A., et al. (1999). The Global Ozone Monitoring Experiment (GOME): Mission Concept and First Scientific Results. *Journal of the Atmospheric Sciences, 56*(2), 151-175.

Demerjian, K. L. (2000). A review of national monitoring networks in North America. *Atmospheric Environment, 34*(12), 1861-1884.

Fei, L., Qiang, Z., Ronald, J. v. d. A., Bo, Z., Dan, T., Liu, Y., et al. (2016). Recent reduction in NO x emissions over China: synthesis of satellite observations and emission inventories. *Environmental Research Letters, 11*(11), 114002.

Fioletov, V. E., McLinden, C. A., Krotkov, N., Li, C., Joiner, J., Theys, N., et al. (2016). A global catalogue of large SO_2 sources and emissions derived from the Ozone Monitoring Instrument. *Atmos. Chem. Phys. Discuss., 2016*, 1-45.

Georgoulias, A. K., van der A, R. J., Stammes, P., Boersma, K. F., & Eskes, H. J. (2018). Trends and trend reversal detection in 2 decades of tropospheric NO_2 satellite observations. *Atmos. Chem. Phys., 2019*, 6269-6294.

Ghude, S. D., Van der A, R. J., Beig, G., Fadnavis, S., & Polade, S. D. (2009). Satellite derived trends in NO2 over the major global hotspot regions during the past decade and their inter-comparison. *Environmental Pollution, 157*(6), 1873-1878.

Hilboll, A., Richter, A., & Burrows, J. P. (2013). Long-term changes of tropospheric NO2 over megacities derived from multiple satellite instruments. *Atmos. Chem. Phys., 13*(8), 4145-4169.

Ingmann, P., Veihelmann, B., Langen, J., Lamarre, D., Stark, H., & Courrèges-Lacoste, G. B. (2012). Requirements for the GMES Atmosphere Service and ESA's implementation concept: Sentinels-4/-5 and -5p. *Remote Sensing of Environment, 120*, 58-69.

Janssens-Maenhout, G., Crippa, M., Guizzardi, D., Dentener, F., Muntean, M., Pouliot, G., et al. (2015). HTAP_v2.2: a mosaic of regional and global emission grid maps for 2008 and 2010 to study hemispheric transport of air pollution. *Atmos. Chem. Phys., 15*(19), 11411-11432.

Jiang, Z., McDonald, B. C., Worden, H., Worden, J. R., Miyazaki, K., Qu, Z., et al. (2018). Unexpected slowdown of US pollutant emission reduction in the past decade. *Proceedings of the National Academy of Sciences*.

Kharol, S. K., Martin, R. V., Philip, S., Boys, B., Lamsal, L. N., Jerrett, M., et al. (2015). Assessment of the magnitude and recent trends in satellite-derived ground-level nitrogen dioxide over North America. *Atmospheric Environment, 118*, 236-245.

Kharol, S. K., McLinden, C. A., Sioris, C. E., Shephard, M. W., Fioletov, V., van Donkelaar, A., et al. (2017). OMI satellite observations of decadal changes in ground-level sulfur dioxide over North America. *Atmos. Chem. Phys., 17*(9), 5921-5929.

Kim, J. (2012). GEMS (Geostationary Environment Monitoring Spectrom- eter) onboard the GeoKOMPSAT to monitor air quality in high temporal and spatial resolution over Asia-Pacific Region. *EGU General Assembly Conference Abstracts*.

Krotkov, N. A., Lamsal, L. N., Celarier, E. A., Swartz, W. H., Marchenko, S. V., Bucsela, E. J., et al. (2017). The version 3 OMI NO2 standard product. *Atmos. Meas. Tech., 10*(9), 3133-3149.

Krotkov, N. A., McLinden, C. A., Li, C., Lamsal, L. N., Celarier, E. A., Marchenko, S. V., et al. (2016). Aura OMI observations of regional SO2 and NO2 pollution changes from 2005 to 2015. *Atmos. Chem. Phys., 16*(7), 4605-4629.

Lamsal, L. N., Duncan, B. N., Yoshida, Y., Krotkov, N. A., Pickering, K. E., Streets, D. G., & Lu, Z. (2015). U.S. NO2 trends (2005–2013): EPA Air Quality System (AQS) data versus improved observations from the Ozone Monitoring Instrument (OMI). *Atmospheric Environment, 110*(Supplement C), 130-143.

Lee, C., Martin, R. V., van Donkelaar, A., O'Byrne, G., Krotkov, N., Richter, A., et al. (2009). Retrieval of vertical columns of sulfur dioxide from SCIAMACHY and OMI: Air mass factor algorithm development, validation, and error analysis. *Journal of Geophysical Research: Atmospheres, 114*(D22), D22303.

Levy, R. C., Munchak, L. A., Mattoo, S., Patadia, F., Remer, L. A., & Holz, R. E. (2015). Towards a long-term global aerosol optical depth record: applying a consistent aerosol retrieval algorithm to MODIS and VIIRS-observed reflectance. *Atmos. Meas. Tech., 8*(10), 4083-4110.

Li, C., Joiner, J., Krotkov, N. A., & Bhartia, P. K. (2013). A fast and sensitive new satellite SO_2 retrieval algorithm based on principal component analysis: Application to the ozone monitoring instrument. *Geophysical Research Letters, 40*(23), 6314-6318.

Li, C., McLinden, C., Fioletov, V., Krotkov, N., Carn, S., Joiner, J., et al. (2017). India Is Overtaking China as the World's Largest Emitter of Anthropogenic Sulfur Dioxide. *Scientific Reports, 7*(1), 14304.

Lin, N., Wang, Y., Zhang, Y., & Yang, K. (2019). A large decline of tropospheric NO2 in China observed from space by SNPP OMPS. *Science of The Total Environment, 675*, 337-342.

Liu, L., Zhang, X., Xu, W., Liu, X., Lu, X., Chen, D., et al. (2017). Estimation of monthly bulk nitrate deposition in China based on satellite NO2 measurement by the Ozone Monitoring Instrument. *Remote Sensing of Environment, 199*, 93-106.

Martin, R. V., Chance, K., Jacob, D. J., Kurosu, T. P., Spurr, R. J. D., Bucsela, E., et al. (2002). An improved retrieval of tropospheric nitrogen dioxide from GOME. *Journal of Geophysical Research: Atmospheres, 107*(D20), 4437.

McLinden, C. A., Fioletov, V., Shephard, M. W., Krotkov, N., Li, C., Martin, R. V., et al. (2016). Space-based detection of missing sulfur dioxide sources of global air pollution. *Nature Geosci, advance online publication*.

Munro, R., Lang, R., Klaes, D., Poli, G., Retscher, C., Lindstrot, R., et al. (2016). The GOME-2 instrument on the Metop series of satellites: instrument design, calibration, and level 1 data processing – an overview. *Atmos. Meas. Tech., 9*(3), 1279-1301.

Myhre, G., Shindell, D., Bréon, F.-M., Collins, W., Fuglestvedt, J., Huang, J., et al. (2013). Anthropogenic and Natural Radiative Forcing. In T. F. Stocker, D. Qin, G.-K. Plattner, M. Tignor, S. K. Allen, J. Boschung, A. Nauels, Y. Xia, V. Bex, & P. M. Midgley (Eds.), *Climate Change 2013: The Physical Science Basis. Contribution of Working Group I to the Fifth Assessment Report of the Intergovernmental Panel on Climate Change* (pp. 659–740). Cambridge, United Kingdom and New York, NY, USA: Cambridge University Press.

National Research Council. (2004). *Climate Data Records from Environmental Satellites*: National Academies Press.

Nowlan, C. R., Liu, X., Chance, K., Cai, Z., Kurosu, T. P., Lee, C., & Martin, R. V. (2011). Retrievals of sulfur dioxide from the Global Ozone Monitoring Experiment 2 (GOME-2) using an optimal estimation approach: Algorithm and initial validation. *Journal of Geophysical Research: Atmospheres, 116*(D18).

Qu, Z., Henze, D. K., Capps, S. L., Wang, Y., Xu, X., Wang, J., & Keller, M. (2017). Monthly top-down NOx emissions for China (2005–2012): A hybrid inversion method and trend analysis. *Journal of Geophysical Research: Atmospheres, 122*(8), 4600-4625.

Richter, A., Begoin, M., Hilboll, A., & Burrows, J. P. (2011). An improved NO2 retrieval for the GOME-2 satellite instrument. *Atmos. Meas. Tech., 4*(6), 1147-1159.

Richter, A., Burrows, J. P., Nüß, H., Granier, C., & Niemeier, U. (2005). Increase in tropospheric nitrogen dioxide over China observed from space. *Nature, 437*, 129.

Schenkeveld, V. M. E., Jaross, G., Marchenko, S., Haffner, D., Kleipool, Q. L., Rozemeijer, N. C., et al. (2017). In-flight performance of the Ozone Monitoring Instrument. *Atmos. Meas. Tech., 10*(5), 1957-1986.

Schneider, P., Lahoz, W. A., & van der A, R. (2015). Recent satellite-based trends of tropospheric nitrogen dioxide over large urban agglomerations worldwide. *Atmos. Chem. Phys., 15*(3), 1205-1220.

Schneider, P., & van der A, R. J. (2012). A global single-sensor analysis of 2002–2011 tropospheric nitrogen dioxide trends observed from space. *Journal of Geophysical Research: Atmospheres, 117*(D16).

Seftor, C. J., Jaross, G., Kowitt, M., Haken, M., Li, J., & Flynn, L. E. (2014). Postlaunch performance of the Suomi National Polar-orbiting Partnership Ozone Mapping and Profiler Suite (OMPS) nadir sensors. *Journal of Geophysical Research: Atmospheres, 119*(7), 4413-4428.

Seinfeld, J. H., & Pandis, S. N. (2016). *Atmospheric Chemistry and Physics: From Air Pollution to Climate Change* (3rd ed.): Wiley.

Streets, D. G., Canty, T., Carmichael, G. R., de Foy, B., Dickerson, R. R., Duncan, B. N., et al. (2013). Emissions estimation from satellite retrievals: A review of current capability. *Atmospheric Environment, 77*, 1011-1042.

Silvern, R. F., Jacob, D. J., Mickley, L. J., Sulprizio, M. P., Travis, K. R., Marais, E. A., et al. (2019). Using satellite observations of tropospheric NO2 columns to infer long-term trends in US NOx emissions: the importance of accounting for the free tropospheric NO2 background. *Atmos. Chem. Phys., 19*(13), 8863-8878.

Sun, K., Zhu, L., Cady-Pereira, K., Chan Miller, C., Chance, K., Clarisse, L., et al. (2018). A physics-based approach to oversample multi-satellite, multispecies observations to a common grid. *Atmos. Meas. Tech., 11*(12), 6679-6701.

Valin, L. C., Russell, A. R., & Cohen, R. C. (2013). Variations of OH radical in an urban plume inferred from NO2 column measurements. *Geophysical Research Letters, 40*(9), 1856-1860.

van der A, R. J., Peters, D. H. M. U., Eskes, H., Boersma, K. F., Van Roozendael, M., De Smedt, I., & Kelder, H. M. (2006). Detection of the trend and seasonal variation in tropospheric NO2 over China. *Journal of Geophysical Research: Atmospheres, 111*(D12).

Veefkind, J. P., Aben, I., McMullan, K., Förster, H., de Vries, J., Otter, G., et al. (2012). TROPOMI on the ESA Sentinel-5 Precursor: A GMES mission for global observations of

the atmospheric composition for climate, air quality and ozone layer applications. *Remote Sensing of Environment, 120*, 70-83.

Wang, S., Zhang, Q., Martin, R. V., Philip, S., Liu, F., Li, M., et al. (2015). Satellite measurements oversee China's sulfur dioxide emission reductions from coal-fired power plants. *Environmental Research Letters, 10*(11), 114015.

Wang, Y., Wang, J., Xu, X., Henze, D. K., Wang, Y., & Qu, Z. (2016). A new approach for monthly updates of anthropogenic sulfur dioxide emissions from space: Application to China and implications for air quality forecasts. *Geophysical Research Letters, 43*(18), 9931-9938.

Weatherhead Elizabeth, C., Reinsel Gregory, C., Tiao George, C., Meng, X. L., Choi, D., Cheang, W. K., et al. (1998). Factors affecting the detection of trends: Statistical considerations and applications to environmental data. *Journal of Geophysical Research: Atmospheres, 103*(D14), 17149-17161.

Yang, K., Carn, S. A., Ge, C., Wang, J., & Dickerson, R. R. (2014). Advancing measurements of tropospheric NO2 from space: New algorithm and first global results from OMPS. *Geophysical Research Letters, 41*(13), 4777-4786.

Yang, K., Dickerson, R. R., Carn, S. A., Ge, C., & Wang, J. (2013). First observations of SO_2 from the satellite Suomi NPP OMPS: Widespread air pollution events over China. *Geophysical Research Letters, 40*(18), 4957-4962.

Zhang, Y., Li, C., Krotkov, N. A., Joiner, J., Fioletov, V., & McLinden, C. (2017). Continuation of long-term global SO_2 pollution monitoring from OMI to OMPS. *Atmos. Meas. Tech., 10*(4), 1495-1509.

Zhou, Y., Brunner, D., Hueglin, C., Henne, S., & Staehelin, J. (2012). Changes in OMI tropospheric NO2 columns over Europe from 2004 to 2009 and the influence of meteorological variability. *Atmospheric Environment, 46*, 482-495.

Zoogman, P., Liu, X., Suleiman, R. M., Pennington, W. F., Flittner, D. E., Al-Saadi, J. A., et al. (2017). Tropospheric emissions: Monitoring of pollution (TEMPO). *Journal of Quantitative Spectroscopy and Radiative Transfer, 186*, 17-39.

Declaration of interests

☒ The authors declare that they have no known competing financial interests or personal relationships that could have appeared to influence the work reported in this paper.

☐The authors declare the following financial interests/personal relationships which may be considered as potential competing interests: